EXTENDED PDF FORMAT
SPONSORED BY

Measuring Cytokines?
Don't Sacrifice on Quality
New ELISA Solutions
>Learn More

www.rndsystems.com

Organotextile Catalysis

Ji-Woong Lee *et al.*

Science **341**, 1225 (2013);
DOI: 10.1126/science.1242196

This copy is for your personal, non-commercial use only.

If you wish to distribute this article to others, you can order high-quality copies for your colleagues, clients, or customers by clicking here.

Permission to republish or repurpose articles or portions of articles can be obtained by following the guidelines here.

The following resources related to this article are available online at www.sciencemag.org (this information is current as of December 9, 2013):

Updated information and services, including high-resolution figures, can be found in the online version of this article at:
http://www.sciencemag.org/content/341/6151/1225.full.html

Supporting Online Material can be found at:
http://www.sciencemag.org/content/suppl/2013/09/11/341.6151.1225.DC1.html

This article **cites 34 articles**, 3 of which can be accessed free:
http://www.sciencemag.org/content/341/6151/1225.full.html#ref-list-1

This article appears in the following **subject collections:**
Chemistry
http://www.sciencemag.org/cgi/collection/chemistry

Downloaded from www.sciencemag.org on December 9, 2013

Science (print ISSN 0036-8075; online ISSN 1095-9203) is published weekly, except the last week in December, by the American Association for the Advancement of Science, 1200 New York Avenue NW, Washington, DC 20005. Copyright 2013 by the American Association for the Advancement of Science; all rights reserved. The title *Science* is a registered trademark of AAAS.

10. C. A. Mirkin, R. L. Letsinger, R. C. Mucic, J. J. Storhoff, *Nature* **382**, 607–609 (1996).
11. S. Y. Park *et al.*, *Nature* **451**, 553–556 (2008).
12. D. Nykypanchuk, M. M. Maye, D. van der Lelie, O. Gang, *Nature* **451**, 549–552 (2008).
13. R. J. Macfarlane *et al.*, *Proc. Natl. Acad. Sci. U.S.A.* **106**, 10493–10498 (2009).
14. M. R. Jones *et al.*, *Nat. Mater.* **9**, 913–917 (2010).
15. M. R. Jones, R. J. Macfarlane, A. E. Prigodich, P. C. Patel, C. A. Mirkin, *J. Am. Chem. Soc.* **133**, 18865–18869 (2011).
16. J. I. Cutler, E. Auyeung, C. A. Mirkin, *J. Am. Chem. Soc.* **134**, 1376–1391 (2012).
17. C. Knorowski, S. Burleigh, A. Travesset, *Phys. Rev. Lett.* **106**, 215501 (2011).
18. B. M. Mladek, J. Fornleitner, F. J. Martinez-Veracoechea, A. Dawid, D. Frenkel, *Phys. Rev. Lett.* **108**, 268301 (2012).
19. M. R. Jones, C. A. Mirkin, *Angew. Chem. Int. Ed.* **52**, 2886–2891 (2013).
20. Y. F. Wang *et al.*, *Nature* **491**, 51–55 (2012).
21. A. G. Dong, X. C. Ye, J. Chen, C. B. Murray, *Nano Lett.* **11**, 1804–1809 (2011).
22. W. H. Evers, H. Friedrich, L. Filion, M. Dijkstra, D. Vanmaekelbergh, *Angew. Chem. Int. Ed.* **48**, 9655–9657 (2009).
23. R. J. Macfarlane *et al.*, *Angew. Chem. Int. Ed.* **49**, 4589–4592 (2010).
24. M. M. Maye, M. T. Kumara, D. Nykypanchuk, W. B. Sherman, O. Gang, *Nat. Nanotechnol.* **5**, 116–120 (2010).
25. Y. Kim, R. J. Macfarlane, C. A. Mirkin, *J. Am. Chem. Soc.* **135**, 10342–10345 (2013).
26. C. N. R. Rao, B. Raveau, *Transition Metal Oxides* (Wiley, New York, ed. 2, 1998).
27. B. L. Ellis, K. T. Lee, L. F. Nazar, *Chem. Mater.* **22**, 691–714 (2010).
28. Materials and methods are available as supporting materials on *Science* Online.
29. K. J. Breslauer, R. Frank, H. Blöcker, L. A. Marky, *Proc. Natl. Acad. Sci. U.S.A.* **83**, 3746–3750 (1986).
30. E. Auyeung *et al.*, *Nat. Nanotechnol.* **7**, 24–28 (2012).
31. X. Ye, J. Chen, C. B. Murray, *J. Am. Chem. Soc.* **133**, 2613–2620 (2011).
32. E. Auyeung, R. J. Macfarlane, C. H. J. Choi, J. I. Cutler, C. A. Mirkin, *Adv. Mater.* **24**, 5181–5186 (2012).
33. I. M. Pryce, K. Aydin, Y. A. Kelaita, R. M. Briggs, H. A. Atwater, *Nano Lett.* **10**, 4222–4227 (2010).
34. C. Zhang *et al.*, *Nat. Mater.* **12**, 741–746 (2013).

Acknowledgments: We thank M. Kanatzidis for helpful discussions regarding the ternary crystal structures synthesized and their corresponding atomic analogs. This material is based on work supported by Air Force Office of Scientific Research awards FA9550-11-1-0275, FA9550-12-1-0280, and FA9550-09-1-0294; Defense Advanced Research Projects Agency award HR0011-13-2-0002; NSF–Materials Research Science and Engineering Center (MRSEC) program DMR-0520513; and the Non-equilibrium Energy Research Center, an Energy Frontier Research Center funded by Department of Energy (DOE), Office of Science, Office of Basic Energy Sciences award DE-SC0000989. M.R.J. acknowledges a Graduate Research Fellowship from NSF; E. A. acknowledges the Department of Defense for a National Defense Science and Engineering Graduate Fellowship. Portions of this work were carried out at the DuPont-Northwestern-Dow Collaborative Access Team (DND-CAT) beamline located at Sector 5 of the Advanced Photon Source (APS). DND-CAT is supported by E. I. DuPont de Nemours & Co., Dow Chemical Company, and the state of Illinois. Use of the APS was supported by the U.S. DOE, Office of Science, Office of Basic Energy Sciences, under contract DE-AC02-06CH11357. The TEM work was carried out in the Electron Probe Instrumentation Center facility of the Northwestern University (NU) Atomic and Nanoscale Characterization Experimental Center, which is supported by NSF–Nanoscale Science and Engineering Center, NSF-MRSEC, Keck Foundation, the state of Illinois, and NU. Ultrathin sectioning was carried out at the NU Biological Imaging Facility, supported by the NU Office for Research.

Supplementary Materials
www.sciencemag.org/cgi/content/full/science.1241402/DC1
Materials and Methods
Supplementary Text
Figs. S1 to S25
Tables S1 to S4
References (*35*, *36*)

3 June 2013; accepted 12 August 2013
Published online 22 August 2013;
10.1126/science.1241402

Organotextile Catalysis

Ji-Woong Lee,[1] Thomas Mayer-Gall,[2] Klaus Opwis,[2]* Choong Eui Song,[3] Jochen Stefan Gutmann,[2,4] Benjamin List[1]*

Throughout human history, textiles have been integral to daily life, but their exploration in catalysis has been rare. Herein, we show a facile and permanent immobilization of organocatalysts on the textile nylon using ultraviolet light. The catalyst and the textile material require no chemical modification for the immobilization. All of the prepared textile-immobilized organocatalysts (a Lewis basic, a Brønsted acidic, and a chiral organocatalyst) display excellent stability, activity, and recyclability for various organic transformations. Very good enantioselectivity (>95:5 enantiomeric ratio) can be maintained for more than 250 cycles of asymmetric catalysis. Practical and straightforward applications of textile organocatalysis may be beneficial for various fields by offering inexpensive and accessible functionalized catalytic materials.

Catalysis with small organic molecules has been intensively investigated in recent years, providing distinct reactivity, activity, and selectivity that complement biocatalysis and transition metal catalysis. Organocatalysts are metal-free and display Lewis acidic or basic and Brønsted acidic or basic reactivity (*1*–*3*). Despite fruitful advancements in academia, further application of organocatalysts in industry is often hampered by their relatively low turnover efficiency, even though exceptions exist. The immobilization of organocatalysts via a covalent bonding interaction could provide a general solution, preventing leaching out of catalytically active centers (*4*–*6*). To access heterogeneous organocatalysts, research has focused on immobilizing the catalysts on diverse solid materials (*7*). However, a general and convenient method for the immobilization of different types of organocatalysts that addresses stability, reactivity, and recyclability of the obtained hetereogeneous material has not been established previously.

We recently became interested in identifying inexpensive and abundant polymeric solid materials that would support organocatalysts while displaying various practical advantages, such as high flexibility, durability, versatility, and broad accessibility. Since the early 1930s, by taking advantage of organic chemistry and polymer technologies, synthetic textiles have been produced on a large scale (*8*). However, chemical applications of textile materials have been rare, possibly because of its perceived inertness for further manipulations. We realized the potential of industrially produced textile materials as support for organic catalysts and now report here the preparation and use of several textile-immobilized organocatalysts, which display excellent activity, selectivity, and recyclability.

Textiles have previously been used as solid supports for nanosized components, such as graphene and carbon nanotubes via physical absorption or adhesion (*9*–*12*). In 1935, Bredig *et al*. used amine-functionalized organic fibers (i.e., cellulose and cotton) as catalysts for a cyanohydrin formation reaction (*13*). Recently, a heterobimetallic complex (Pd/Co) was prepared by using wool as a ligand and applied in asymmetric hydration of unsaturated carboxylic acids (*14*). However, as of yet textile materials have not been used as a general solid support for organic compounds in selective catalysis. During our own research, we have found that the irradiation of textiles can result in the photochemical production of surface radicals, which can be used to further functionalize the textile with organic molecules and biocatalysts (*15*–*17*). Therefore, we presumed that this strategy could be applied in a facile preparation of solid-supported organocatalysts under photochemical reaction conditions.

We commenced our study by investigating the immobilization of three representative organocatalysts, a dimethylaminopyridine (DMAP) derivative, a sulfonic acid, and a bifunctional chiral organocatalyst, using nylon as support (Fig. 1). Gratifyingly, all organocatalysts (**1a**, **2**, and **3**) were successfully immobilized on the textile and fully analyzed by various methods (see tables S1 to S5 for immobilization reaction conditions). The catalyst loading can be controlled by adding a cross-linker, such as PETA (penta-erythritol triacrylate) (*18*). Lewis basic catalyst **1a**, Brønsted acid catalyst **2**, and bifunctional organocatalyst **3a**, which possesses both a basic and an acidic functionality, were equally tolerated under the

---

[1]Max-Planck-Institut für Kohlenforschung, Kaiser-Wilhelm-Platz 1, 45470 Mülheim an der Ruhr, Germany. [2]Deutsches Textilforschungszentrum Nord-West gGmbH, Adlerstraße 1, 47798 Krefeld, Germany. [3]Department of Chemistry, Sungkyunkwan University, 300 Cheoncheon, Jangan, Suwon, Gyeonggi, 440-746, Korea. [4]Institute of Physical Chemistry and CENIDE (Center for Nanointegration), University Duisburg-Essen, Universitätsstraße 5, 45117 Essen, Germany.

*Corresponding author. E-mail: opwis@dtnw.de (K.O.); list@kofo.mpg.de (B.L.)

photochemical reaction conditions yielding textile catalysts **OrganoTexCat-1a**, **-2** and **-3a** with catalyst loadings of up to 0.025 mmol/g. Irradiation time proved critical for both catalyst loading and catalytic activity (vide infra). A short irradiation time (5 min) for each side of the textile could improve the catalyst loading while preventing any degradation of the textile and the organic catalysts.

Next, the catalytic activity and recyclability of catalyst **OrganoTexCat-1a** was investigated in the acylation reaction of sterically demanding phenol **4** with isobutyric anhydride (Fig. 2A) (*19*). In the absence of catalyst **OrganoTexCat-1a** or in the presence of blank polyamide instead of **OrganoTexCat-1a**, only insignificant background reaction was observed under otherwise identical reaction conditions. After full conversion of starting material **4**, the catalyst was easily recovered by decanting the liquid phase, simply washing with an organic solvent, and drying by blowing air onto the textile. Several recycling experiments revealed the robustness of our catalyst **OrganoTexCat-1a** (Fig. 2B). In more than 10 recycling experiments, no significant erosion of the catalytic activity was observed. The catalyst can be deactivated by forming an acid-base salt with the carboxylic acid by-product of the reaction (fourth run in Fig. 2B). However, the catalytic activity could be readily recovered by washing with triethylamine to regenerate the catalyst with good activity.

In addition to **OrganoTexCat-1**, we prepared several other textile-supported DMAP variants with different linker groups (fig. S4). These Lewis ba-

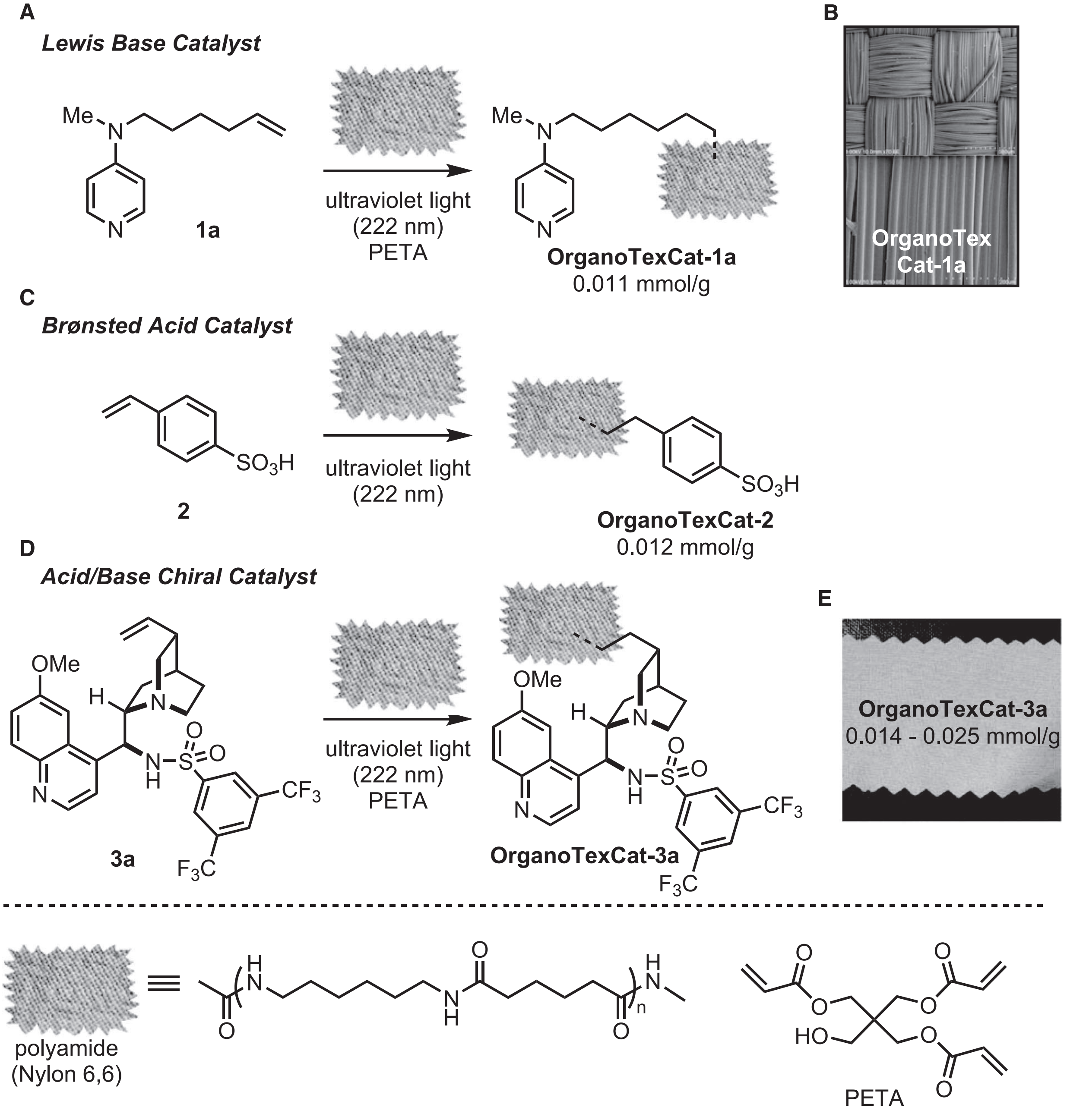

Fig. 1. Reaction conditions for the photochemical immobilization. The textile was irradiated with ultraviolet light for 5 min on each side of the textile wetted by a solution of the organic catalyst. (**A**) Immobilization of DMAP derivative **1a** on textile from an acetonitrile solution. The catalyst loading was determined by acid/base titration. Me, methyl group. (**B**) Scanning electron microscope image of **OrganoTexCat-1a**. (**C**) Immobilization of *p*-styrenesulfonic acid (**2**) on textile from a water/ethanol (1:1) solution. The catalyst loading was determined by elemental analysis. (**D**) Immobilization of bifunctional chiral catalyst **3** on textile from an acetonitrile solution. Catalyst loading was determined by elemental analysis, MAS (magic-angle solid-state) ^{19}F NMR spectroscopy (fig. S1), and XPS analysis (figs. S2 and S3). (**E**) A photograph of catalyst **OrganoTexCat-3a** (numbers indicate the catalyst loading per gram of sheet).

sic catalysts can also be used in a carbonate-forming reaction from epoxide **6** (*20*). **OrganoTexCat-1d**, which showed the highest activity after optimization of the side chain structure, demonstrated reasonable activity for this reaction in supercritical CO_2 (Fig. 2C). **OrganoTexCat-1d** could be easily recycled and showed identical activity for seven cycles affording cyclic carbonate **7** without considerable formation of polymeric by-products. This result highlights the high stability of the catalyst under high pressure (100 atm) and temperatures (up to 75°C), which might be beneficial for further applications.

Highly Brønsted acidic heterogeneous catalysts are of great interest in industrial chemical production (*21*). As shown in Fig. 2D, acidic **OrganoTexCat-2** displays good activity in an intramolecular hydroetherification, affording the corresponding tetrahydrofuran in excellent yield. No background reaction was observed in the absence of the catalyst. The immobilized acidic catalyst is easy to handle and features robust stability for the transformation, which are the primary advantages of polymer-supported catalysts.

After establishing a facile immobilization methodology for organocatalysts on textile materials and applying them successfully to three different classes of transformations, we turned our attention to asymmetric catalysis. Although various attempts have been made to provide heterogeneous chiral organocatalysts, they typically give inferior stereoselectivity, possibly because of the alteration of the microenvironment of the catalytically active sites (*22*, *23*).

Cinchona alkaloids, naturally occurring chiral molecules with various functional groups, have emerged as privileged ligands and organocatalysts for various catalytic asymmetric transformations (*24*). With *cinchona*-sulfonamide–based **OrganoTexCat-3a** in our hands, we evaluated activity and recyclability by performing the alcoholytic desymmetrization of cyclic anhydride **10** (*25*–*27*). **OrganoTexCat-3a** showed a very similar enantioselectivity [96.5:3.5 enantiomeric ratio (er)] to homogeneous catalyst **3a** (97:3 er) although requiring a somewhat longer reaction time (Fig. 3A).

After the photochemical preparation of catalyst **OrganoTexCat-3a**, residual homogenous catalyst **3a** could be recovered and reused for subsequent immobilization reactions (figs. S5 and S6). Furthermore, the robustness of **OrganoTexCat-3a** is illustrated with hundreds of recycling experiments (Fig. 3B). By varying the reaction conditions, such as the amount of nucleophile and the concentration of the substrate, we obtained an optimal enantioselectivity (er up to 97:3). This result is comparable to the homogeneous reaction conditions with 5 to 10 mole percent (mol %) of catalyst loading of **3a**. Moreover, the catalyst loading could be decreased to 4 mol % without loss of enantioselectivity (77th to 81st cycles). To investigate the fate of our catalyst, we conducted further recycling experiments by using 6 mol % of the catalyst, and the desired product was obtained with more than 95:5 er without erosion of enantioselectivities for more than 220 cycles. After 200 cycles, a slight deactivation of **OrganoTexCat-3a** was observed and resulted in a lower enantioselectivity (94:6 er). However, increasing the catalyst loading to 10 mol % led to an increase of the enantioselectivity back to 95:5 er (231st cycle). Therefore, we concluded that the chemical structure of the chiral catalyst was indeed intact. The loss of activity and enantioselectivity could be ascribed to the detachment of a certain amount of the catalytically active species from the textile after more than 300 recycling experiments in the presence of excess of methanol.

The substrate scope of **OrganoTexCat-3a** for the desymmetrization of different *meso*-anhydrides has also been determined and is summarized in Fig. 4A. Various *meso*-anhydrides were smoothly transformed into enantioenriched hemiesters with excellent yields (up to 99%) and enantioselectivities (er up to 97:3). Bi- and tricyclic compounds could also be used to afford the desired products with high enantioselectivities and comparable selectivity to the homogeneous catalysis conditions. Moreover, product **11h**, a valuable precursor of statin derivatives (*27*), could be obtained on a gram scale by using a flow reactor with an **OrganoTexCat-3a** packed column in an iterative continuous reaction (Fig. 4B). The column was prepared without any sophisticated packing procedure, contrary to powder- or resin-based heterogeneous catalysts. The textile material showed

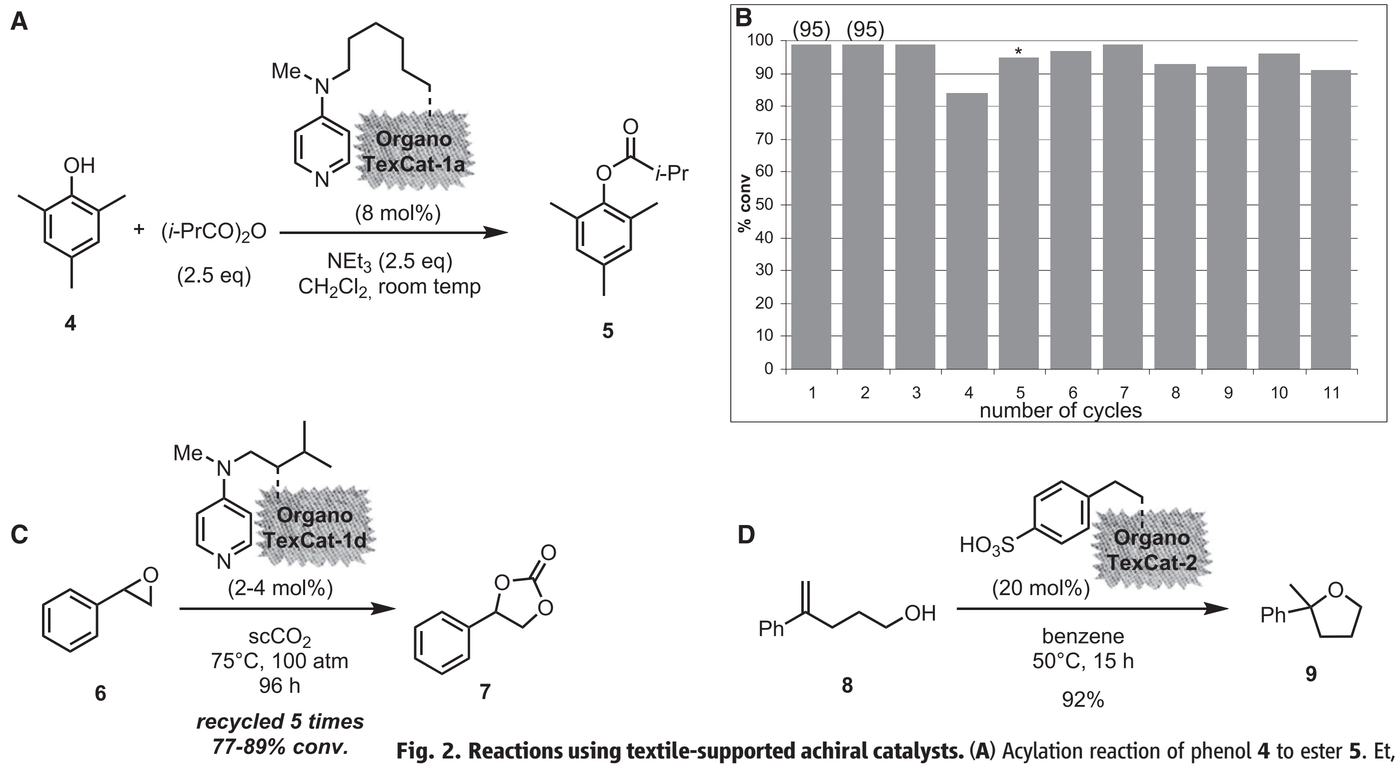

Fig. 2. Reactions using textile-supported achiral catalysts. (**A**) Acylation reaction of phenol **4** to ester **5**. Et, ethyl group; Ph, phenyl group; *i*-Pr, isopropyl; eq, equivalent. (**B**) Recycling experiments of **OrganoTexCat-1a** (reaction conditions: 8 mol % of catalyst loading, 36 hours in CH_2Cl_2, [4] = 0.05 M). The numbers in the parentheses are isolated yields of the acylated product. *After the fourth cycle, each experiment was conducted with the triethylamine-washed textile catalyst. (**C**) A carbonate-forming reaction catalyzed by **OrganoTexCat-1d**. $scCO_2$ indicates supercritical CO_2 reaction conditions. (**D**) A hydroetherification reaction using acidic **OrganoTexCat-2**.

good absorption ability for organic solvents, which can facilitate mass transfer onto the material, generating a microfluidic environment via capillary action to increase the effective catalyst concentration. As shown in Fig. 4C, enantioenriched product **11h** was obtained in quantitative yield (>99% yield) and excellent enantioselectivity (up to 97:3 er) by taking advantage of a simple fixed-bed reactor setup (*28*, *29*). After full conversion of the starting material, the column was washed with methyl *tert*-butyl ether (MTBE) and reused 10 times, showing identical activity and enantioselectivity.

In addition to the robustness of our organotextile catalysts, several aspects should be highlighted. Compared with polymer films, textile fibers exhibit a much higher surface area. The inherent capillary action of textiles allows an easy and uniform wetting of the material with the catalyst before the photoinduced immobilization. This leads to a uniform three-dimensional coating. Moreover, the active surface area is easily adjustable by varying the fiber diameter, which should ultimately enable preparation of organotextiles with significantly higher catalyst loadings. The flexible construction of fabrics allows reactor constructions of arbitrary geometry and a quick removal of the catalyst. Our results underscore the vast potential of supported organocatalysts for chemical synthesis (*30*).

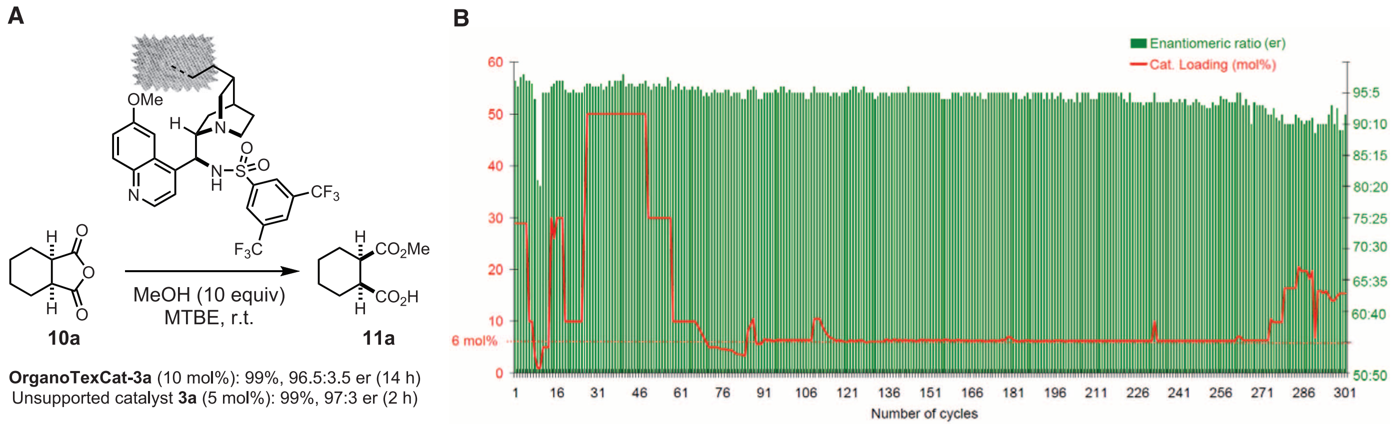

Fig. 3. Performance of the textile-supported chiral catalyst. (**A**) Comparison of the activity of homogeneous catalyst **3a** and heterogeneous **OrganoTexCat-3a**. r.t., room temperature. (**B**) Recycling experiments. For experimental details, see table S6.

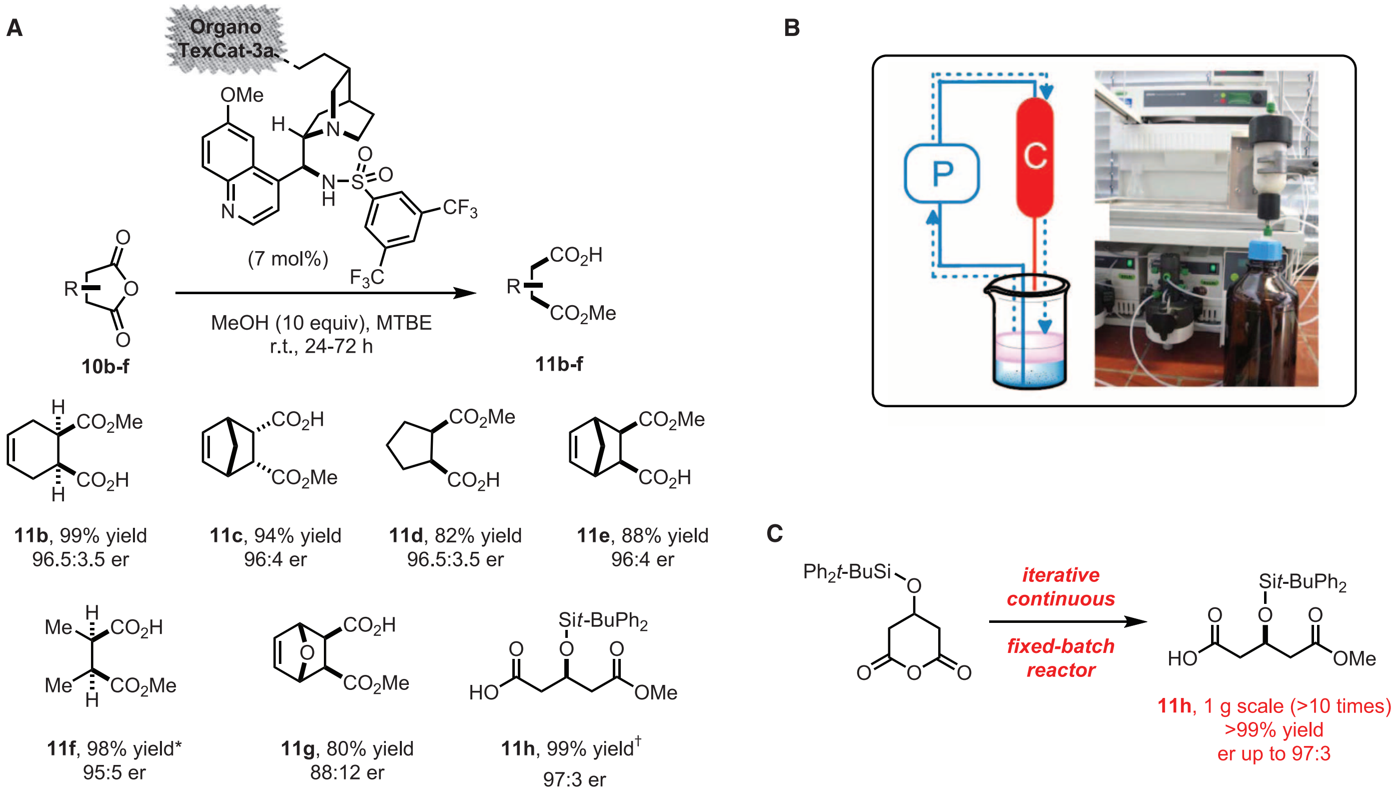

Fig. 4. Substrate scope and applications of OrganoTexCat-3a. (**A**) Substrate scope of the desymmetrization of anhydrides **10** catalyzed by textile **OrganoTexCat-3a**. *15 mol % of catalyst **OrganoTexCat-3a** was used. †50 mol % of catalyst **OrganoTexCat-3a** was used. (**B**) Schematic illustration of the continuous circle reactor and the picture of the reaction setup. P, pump; C, column packed with **OrganoTexCat-3a**. (**C**) Desymmetrization of silylated glutamic anhydride; see table S7 and fig. S7 for the optimization of reaction conditions. *t*-Bu, tertbutyl.

References and Notes

1. T. P. Yoon, E. N. Jacobsen, *Science* **299**, 1691–1693 (2003).
2. B. List, J. W. Yang, *Science* **313**, 1584–1586 (2006).
3. D. W. C. MacMillan, *Nature* **455**, 304–308 (2008).
4. M. Benaglia, A. Puglisi, F. Cozzi, *Chem. Rev.* **103**, 3401–3430 (2003).
5. F. Cozzi, *Adv. Synth. Catal.* **348**, 1367–1390 (2006).
6. T. E. Kristensen, T. Hansen, *Eur. J. Org. Chem.* **2010**, 3179–3204 (2010).
7. B. Merrifield, "Nobel lecture: Solid phase synthesis" (Nobel Foundation, Stockholm, 1984); available online at www.nobelprize.org/nobel_prizes/chemistry/laureates/1984/merrifield-lecture.html.
8. W. H. Carothers, U.S. Patent 2,130,523 (1938).
9. L. B. Hu *et al.*, *Nano Lett.* **10**, 708–714 (2010).
10. M. Pasta, F. La Mantia, L. B. Hu, H. D. Deshazer, Y. Cui, *Nano Res.* **3**, 452–458 (2010).
11. G. H. Yu *et al.*, *Nano Lett.* **11**, 2905–2911 (2011).
12. M. D. Lima *et al.*, *Science* **331**, 51–55 (2011).
13. G. Bredig, F. Gerstner, H. Lang, *Biochem. Z.* **282**, 88 (1935).
14. S. Q. Wang *et al.*, *J. Mol. Catal. Chem.* **264**, 60–65 (2007).
15. D. Praschak, T. Bahners, E. Schollmeyer, *Appl. Phys. A* **66**, 69–75 (1998).
16. S. L. Gao *et al.*, *Appl. Phys. B* **81**, 681–690 (2005).
17. K. Opwis, D. Knittel, E. Schollmeyer, *Biotechnol. J.* **2**, 347–352 (2007).
18. C. Decker, *Polym. Int.* **51**, 1141–1150 (2002).
19. A. Sakakura, K. Kawajiri, T. Ohkubo, Y. Kosugi, K. Ishihara, *J. Am. Chem. Soc.* **129**, 14775–14779 (2007).
20. M. North, R. Pasquale, C. Young, *Green Chem.* **12**, 1514 (2010).
21. T. Okuhara, *Chem. Rev.* **102**, 3641–3666 (2002).
22. C. Bleschke, J. Schmidt, D. S. Kundu, S. Blechert A. Thomas, *Adv. Synth. Catal.* **353**, 3101–3106 (2011).
23. C. A. Wang *et al.*, *Chem. Eur. J.* **18**, 6718–6723 (2012).
24. C. E. Song, Ed., *Cinchona Alkaloids in Synthesis and Catalysis* (Wiley-VCH, Weinheim, Germany, 2009).
25. S. H. Oh *et al.*, *Angew. Chem. Int. Ed.* **47**, 7872–7875 (2008).
26. S. H. Youk *et al.*, *Chem. Commun.* **2009**, 2220–2222 (2009).
27. S. E. Park *et al.*, *Adv. Synth. Catal.* **352**, 2211–2217 (2010).
28. N. G. Anderson, *Org. Process Res. Dev.* **16**, 852–869 (2012).
29. L. B. Datsevich, in *Conventional Three-Phase Fixed-Bed Technologies*, L. B. Datsevich, Ed. (Springer, New York, 2012), pp. 7–9.
30. S. V. Ley *et al.*, *J. Chem. Soc. Perkin Trans. 1* **2000**, 3815–4195 (2000).

Acknowledgments: Generous support by Max Planck Society, DECHEMA (Gesellschaft für Chemische Technik und Biotechnologie e.V.), AIF (Arbeitsgemeinschaft Industrieller Forschungsvereinigungen "Otto von Guericke" e.V.)/IGF (Industrielle Gemeinschaftsforschung) 436 ZN, the Ministry of Education (Priority Research Centers Program, Republic of Korea), and the European Research Council (Advanced Grant "High Performance Lewis Acid Organocatalysis, HIPOCAT") are gratefully acknowledged. We thank our analytical departments [mass spectroscopy, x-ray photoelectron spectroscopy (XPS analysis), nuclear magnetic resonance (NMR) spectroscopy, and high-performance liquid chromatography analysis] for excellent assistance. The authors have filed a patent on the methods presented herein.

Supplementary Materials

www.sciencemag.org/cgi/content/full/341/6151/1225/DC1
Materials and Methods
Supplementary Text
Figs. S1 to S8
Tables S1 to S8
Supplementary Data
References (*31*–*38*)

20 June 2013; accepted 5 August 2013
10.1126/science.1242196

Slow Earthquakes, Preseismic Velocity Changes, and the Origin of Slow Frictional Stick-Slip

Bryan M. Kaproth and C. Marone

Earthquakes normally occur as frictional stick-slip instabilities, resulting in catastrophic failure and seismic rupture. Tectonic faults also fail in slow earthquakes with rupture durations of months or more, yet their origin is poorly understood. Here, we present laboratory observations of repetitive, slow stick-slip in serpentinite fault zones and mechanical evidence for their origin. We document a transition from unstable to stable frictional behavior with increasing slip velocity, providing a mechanism to limit the speed of slow earthquakes. We also document reduction of *P*-wave speed within the active shear zone before stick-slip events. If similar mechanisms operate in nature, our results suggest that higher-resolution studies of elastic properties in tectonic fault zones may aid in the search for reliable earthquake precursors.

Slow earthquakes represent one mode of the spectrum of fault slip behaviors ranging from steady aseismic slip at plate tectonic rates (a few millimeters per year) to normal earthquakes with rupture propagation at a few kilometers per second and fault slip speeds of 1 to 10 m/s, which is consistent with elastodynamic theory (*1*–*6*). Like normal earthquakes, slow earthquakes can accommodate most of a fault's slip budget, with equivalent magnitudes of 8 or larger; yet, this slip occurs slowly, over days to years, rather than the few tens of seconds for normal earthquakes (*1*–*4*). Slow earthquakes often occur adjacent to traditional seismogenic zones (*5*, *7*) and may load these earthquake-prone areas. Moreover, recent work suggests that slow earthquakes may abet potentially devastating earthquakes, such as the 2011 M_w 9 Tohoku Oki earthquake (*7*), and thus, understanding the physics of slow earthquakes and identifying possible precursory changes in fault zone properties are increasingly important goals.

Although observations of slow earthquakes abound, the underlying processes that produce these self-sustaining, quasi-dynamic ruptures remain poorly understood (*3*–*8*). A particularly vexing aspect of slow earthquakes is the mechanism that limits slip speed yet allows self-sustained rupture propagation. One possibility is that slow earthquakes represent prematurely arrested normal earthquakes with slip-speed limited by a mechanism such as dilatant hardening or a transition in friction constitutive behavior with increasing slip speed. Several mechanisms have been proposed (*4*–*12*), but the origin of slow earthquakes remains elusive. Additionally, if slow earthquakes initiate like normal earthquakes they may exhibit precursory effects, such as accelerating fault slip or changes in elastic wave-speed within the rupture nucleation region.

Here, we describe laboratory observations of fault-zone materials showing repetitive, slow stick-slip friction events that are reminiscent of slow earthquakes (Fig. 1). We sheared layers of lizardite-rich serpentinite at constant normal stress of 1 MPa (supplementary text). Each experiment includes 50+ stick-slip events, with durations ranging up to 35 s (Fig. 2). Our experiments show that the laboratory fault zones undergo a transition from velocity-weakening to velocity-strengthening friction behavior above slip rates of ~10 μm/s (Fig. 3). During each slip event, the fault zone shows large changes in elastic wave speed (2 to 21% decrease), with precursory changes of 1 to 3% starting up to 60 s before failure (Fig. 4).

Like natural earthquakes, fault slip velocity during stick-slip events exceeded the imposed far-field velocity. The full record for one experiment shows the character of stress drops and the corresponding stair-step pattern of fault displacement (Fig. 1A). Stick-slip events have durations of 1 to 35 s, average slip velocities of 15 to 280 μm/s, average displacements of 10 to 900 μm, and evolve from small to large events with increasing shear (Fig. 1B). We observed slow stick-slip events at a range of loading velocities (Fig. 2). Each event generally released tens of kilopascals of shear stress—roughly a 5 to 10% stress drop (Fig. 1A). Maximum slip velocities ranged from 60 to 1300 μm/s, but peak velocities were generally sustained for <1 s, with longer acceleration and deceleration periods (Fig. 2B). The events resemble results from experiments conducted on halite (*12*) but are distinguished by their consistent, repetitive nature.

To investigate the processes responsible for these slow-slip events, we conducted additional experiments under stiff loading conditions, including slide-hold-slide (SHS) (fig. S2) and velocity-step tests (fig. S3). We determined the friction rate parameter (a-b = $\Delta\mu/\Delta lnV$, where V is the velocity) and critical slip distance (D_c) using standard techniques (*13*). With increased shear strain and hold time, (a-b) generally decreased, and D_c increased (fig. S2A). At slip velocities

---

Department of Geosciences, and Energy Institute Center for Geomechanics, Geofluids and Geohazards, Pennsylvania State University, University Park, PA 16802, USA.